Chem Biol Drug Des 2016; **88:** 43–53

Research Article

Synthesis, Biological Evaluation, and Molecular Docking of 8-imino-2-oxo-2*H*,8*H*-pyrano[2,3-*f*]chromene Analogs: New Dual AChE Inhibitors as Potential Drugs for the Treatment of Alzheimer's Disease

Jeelan Basha Shaik[1], Bhagath Kumar Palaka[2], Mohan Penumala[1], Siddhartha Eadlapalli[3], Manidhar Darla Mark[4], Dinakara Rao Ampasala[2], Ramakrishna Vadde[3] and Damu Amooru Gangaiah[1,*]

[1]Department of Chemistry, Yogi Vemana University, Kadapa, India
[2]Centre for Bioinformatics, School of life Sciences, Pondicherry Central University, Puducherry, India
[3]Department of Biotechnology and Bioinformatics, Yogi Vemana University, Kadapa, India
[4]Department of Chemistry, University College of Sciences, Sri Venkateswara University, Tirupati, India
**Corresponding author: Damu Amooru Gangaiah, agdamu01@gmail.com*

Alzheimer's disease onset and progression are associated with the dysregulation of multiple and complex physiological processes, and a successful therapeutic approach should therefore address more than one target. In line with this modern paradigm, a series of 8-imino-2-oxo-2*H*,8*H*-pyrano[2,3-*f*]chromene analogs (4a–q) were synthesized and evaluated for their multitarget-directed activity on acetylcholinesterase, butyrylcholinesterase (BuChE), 2,2'-azino-bis(3-ethylbenzthiazoline-6-sulfonic acid) (ABTS) radical, and amyloid-β peptide (Aβ) specific targets for Alzheimer's disease therapy. Most of the synthesized compounds showed remarkable acetylcholinesterase inhibitory activities in low nM concentrations and good ABTS radical scavenging activity, however, no evidence of BuChE inhibitory activity. Among them, 3-bromobenzylamide derivative 4m exhibited the best acetylcholinesterase inhibitory activity with IC_{50} value of 13 $\pm$ 1.4 nM which is 51-fold superior to galantamine, a reference drug. Kinetic and molecular docking studies indicated 4m as mixed-type inhibitor, binding simultaneously to catalytic active and peripheral anionic sites of acetylcholinesterase. Five compounds 4e, 4f, 4g, 4j, and 4k have shown 1.4- to 2.5-fold of higher antioxidant activities than trolox. Interestingly, the most active compound 4m demonstrated dosage-dependent acceleration of Aβ_{1-42} aggregation, which may reduce toxicity of oligomers. Overall, these results lead to discovery of fused tricyclic coumarins as promising dual binding site inhibitors of acetylcholinesterase and afford multifunctional compounds with potential impact for further pharmacological development in Alzheimer's therapy.

Key words: acetylcholinesterase, Alzheimer's disease, antioxidant, Aβ_{1-42} aggregation, butyrylcholinesterase, coumarin, docking, Kinetic study

Received 6 August 2015, revised 18 December 2015 and accepted for publication 10 January 2016

Neurodegenerative diseases (NDs) are, along with cancer and cardiovascular diseases, the most important cause of illness and death in developed countries. The high social and clinical costs of health care and assistance for ND suffering patients are exasperated by the lack of disease-modifying therapies. Despite the wide efforts of both academic and industrial researchers, there are still only a few pharmacological treatments for NDs (1). In the vast plethora of NDs, Alzheimer's disease (AD) stands out as the most common form of dementia in the elderly population with an insidious onset and a chronic progression. With the progression of disease, the prominent indications are the continuous memory loss, confusion, petulance, anger and the lack of vigor in body to function evenly which eventually become the ultimate cause of death (2). According to the World Alzheimer Report 2015, currently, over 46 million people around the world live with dementia conditions and the number is expected to nearly double every 20 years, resulting in more than 131.5 million in 2050 if no efficient treatment is discovered (3).

In the past decade, treatment strategies for AD have mainly been aimed at improving cholinergic neurotransmission in the brain, which were mostly based on the 'cholinergic hypothesis'. Concerning the cholinergic hypothesis, one of the rational and effective approaches to treat the AD's symptoms is raising the acetylcholine (ACh) through inhibition of acetylcholinesterase (AChE) that is responsible for hydrolysis of ACh in presynaptic areas (4). Although AChE inhibitors have become the mainstays for treating

 doi: 10.1111/cbdd.12732

AD, the non-selectivity of these drugs, poor bioavailability, adverse cholinergic side-effects in the periphery, narrow therapeutic ranges and hepatotoxicity are some of the severe limitations to their therapeutic success (5).

Recent research has demonstrated that oxidative stress plays a key role in initiating the aggregation of Aβ and tau protein hyperphosphorylation, involved in the early stage of the pathologic cascade of AD (6). Therefore, drugs aimed at clearing or preventing the formation of the free radicals may be useful for either the prevention or effective treatment of AD. Because AChE as well as oxidative stress are important targets for the treatment of AD, some studies have been devoted to searching multifunctional agents that act on both AChE and oxidative stress and proved that the combination of AChE inhibition and antioxidant is an effective strategy for developing new multifunctional drugs for AD treatment (7).

The 4-kDa (40–42-amino acid) amyloid-β peptide (Aβ) is derived from the amyloid precursor protein (APP) through sequential proteolysis (8). According to amyloid cascade hypothesis, progressive accumulation of Aβ aggregates is widely believed to be fundamental to the initial development of neurodegenerative pathology and to trigger a cascade of events such as neurotoxicity, oxidative damage, and inflammation that contribute to the progression of AD (9–12). The aggregation of soluble Aβ monomer or oligomers into insoluble plaques or amyloid fibrils is a crucial step. A fibrillization involves formation of dimers and small oligomers followed by growth into protofibrils and fibrils via a complex multistep-nucleated polymerization. It is also reported that the oligomers of amyloid peptides are more toxic to neurons in comparison with the fibril aggregates. To reduce the cytotoxicity of these peptides, two kinds of strategies, that is, inhibiting aggregation and disassembling aggregates of amyloid peptides by a variety of designed molecules such as peptides, antibodies, metal ion chelators, small molecules, and nano particles are applied (13–17). Currently, smart self-assembling molecules have been identified that associate and promote the peptide–peptide and peptide–organic interactions converting the Aβ monomers and oligomers into non-toxic forms, which is a different non-destructive approach as compared to inhibiting the aggregation of peptides (18,19).

Structural development of AChE inhibitors resulted in introducing naturally occurring as well as the synthetic coumarin analogs as potent AChE inhibitors (20,21). Previous studies have demonstrated that coumarin motif can bind primarily to the PAS of AChE and amine functional moieties linked to coumarin using appropriate spacer interact with CAS of AChE and thus act as dual binding site inhibitors (22–24). Furthermore, functionalization of the aromatic center of coumarins has led to development of novel analogs that are capable of inhibiting Aβ aggregation and provide protection to neurons against Aβ-induced oxidative stress and free radicals (25). Actually, coumarin scaffold represents a widely occurring, nature friendly privileged structure, whose functionalization is straightforward. These facts have made coumarins as interesting molecules for drug discovery in the field of AChE inhibitors.

Following these reasons, a series of seventeen new fused tricyclic coumarin derivatives bearing varied amide moieties were synthesized. The inhibitory effects on AChE and BuChE, kinetics of inhibition and molecular docking study of compounds, were investigated. In addition, an *in vitro* ABTS radical scavenging activity and accelerating activity of Aβ aggregation process was tested.

Methods and Materials

For the synthesis, starting materials and reagents were commercially purchased and used without further purification. All synthetic compounds were confirmed by ESI mass analysis, FT-IR, ^{1}H and ^{13}C NMR spectra. Acetylcholinesterase (EC 3.1.1.7, from Electric eel), butyrylcholinesterase (EC 3.1.1.8, from Horse serum), 2,2'-azino-bis(3-ethylbenzthiazoline-6-sulfonic acid) (ABTS), β-amyloid$_{1-42}$ (Aβ_{1-42}), thioflavin T, 5,5'-dithio-bis(2-nitrobenzoic acid) (DTNB), acetylthiocholine iodide, butyrylthiocholine iodide, galantamine and trolox were purchased from Sigma-Aldrich (St. Louis, MO, USA).

General

Reaction progress was monitored using analytical thin layer chromatography (TLC) on precoated silica gel 60 F_{254} aluminum plates, and the spots were detected under UV light (254 nm). Melting points were measured on an electrically heated melting point apparatus and were uncorrected. The IR spectra were taken as KBr disks using Perkin Elmer Spectrum 2 spectrophotometer (Singapore). The NMR spectra were recorded on a Bruker spectrometer (Avance II, Switzerland) operating at 400 MHz (^{1}H) and at 100 MHz (^{13}C). The chemical shifts (δ) and coupling constants (J) are expressed in parts per million and hertz, respectively. Splitting patterns are designated as s, singlet; d, doublet; t, triplet; m, multiplet. The atoms numbering of target compounds used for NMR data are depicted in Scheme 1. Mass spectra were determined with a 70 eV (ESI probe) on an Agilent LC/MSD trap SL 1100 series spectrometer (Agilent Technology, California, USA).

Procedure for the preparation of 7-hydroxy coumarin (1)

To a mixture of resorcinol 3 g (27 mmol) and DL-Malic acid 2.46 g (18 mmol) in a round-bottom flask (100 mL), sulfuric acid (6.1 mL) was added slowly at room temperature. The reaction mixture was stirred at 120 °C for 2 h, cooled to room temperature, and then, it was slowly poured into crushed ice. The resulting solid was separated by filtration and washed successively with water (26). The

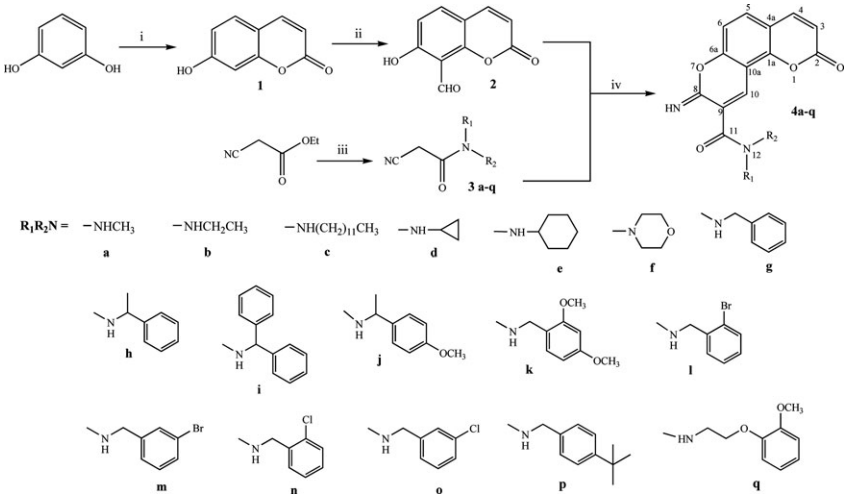

Scheme 1: Synthetic pathway of 8-imino-2-oxo-2H,8H-pyrano[2,3-*f*]chromene derivatives (**4a**–**q**) Reagents and conditions: (i) DL-malic acid, H_2SO_4, 120 °C, 2 h (ii) HMTA, glacial acetic acid, 90 °C, reflux, 6 h (iii) corresponding amine (iv) Et_3N, EtOH.

product was dried and recrystallized with ethanol to get compound **1**.

Synthetic procedure for 7-hydroxy-8-formylcoumarin (2)

7-Hydroxycoumarin **1** (20.0 g, 0.123 mol) and hexamethylenetetramine (40.0 g, 0.285 mol) were added to glacial acetic acid (150 mL) and stirred at 90 °C for 6 h. Thereafter, aqueous solution of HCl (300 mL, conc. HCl/H_2O = 84:100, v/v) was added and heated under reflux at 70 °C for 30 min. After cooling, mixture was poured into ice water (1500 mL) and exhaustively extracted with ethyl acetate. The combined organic extracts were dried over Na_2SO_4, and the solvent was removed under reduced pressure (27). The crude solid was purified by crystallization from ethanol.

General procedure for the synthesis of N-substituted cyano acetamide derivatives (3a–q)

A solution of different amines (1 mmol) and ethylcyanoacetate (1.2 mmol) was stirred at room temperature in an easily available screw cap bottle (28,29). The amide, in most cases, typically precipitated after some minutes to hours. Formed product was filtered and washed several times with ether to obtain pure N-substituted cyanoacetamide derivatives **3a**–**q**.

General synthetic procedure for preparation of final product: (4a–q)

To a solution of 7-hydroxy-8-formylcoumarin **2** (1.5 mmol) and (**3a**–**q**) (3.1 mmol) in ethanol (10 mL) was added Et_3N (0.1 mmol) drop wise at room temperature. The resulting mixture was heated to reflux temperature for 2–3 h and then allowed to cool to room temperature (30). The product precipitated from the reaction mixture was collected by filtration and washed with cold methanol (2–3 mL) to yield corresponding final product (**4a**–**q**).

8-imino-N-methyl-2-oxo-2H,8H-pyrano[2,3-f] chromene-9-carboxamide (4a)

Orange red solid; yield: 71%; mp: 215–217 °C; IR (KBr): *v* 3435, 3308 (N–H), 2939, 2856, 1746 (C=O), 1683 (C=N), 1617 (C=O) cm^{-1}; ^1H NMR (400 MHz, $CDCl_3$): δ 9.92 (brs, 1H, 12-NH), 9.01 (s, 1H, 10-H), 7.74 (brs, 1H, 8-NH), 7.67 (d, 1H, *J* = 9.2 Hz, 4-H), 7.53 (d, 1H, *J* = 8.4 Hz, 5-H), 7.03 (d, 1H, *J* = 8.4 Hz, 6-H), 6.41 (d, 1H, *J* = 9.2 Hz, 3-H), 3.00 (d, 3H, *J* = 4.8 Hz, 1'-CH_3); ESI-MS (*m/z*): 271 $(M+H)^+$.

N-ethyl-8-imino-2-oxo-2H,8H-pyrano[2,3-f] chromene-9-carboxamide (4b)

Orange red solid; yield: 62%; mp: 174–176 °C; IR (KBr): *v* 3454, 3320 (N–H), 2925, 1745 (C=O), 1672 (C=N), 1615 (C=O) cm^{-1}; ^1H NMR (400 MHz, $CDCl_3$): δ 9.97 (brs, 1H, 12-NH), 8.91 (s, 1H, 10-H), 7.77 (brs, 1H, 8-NH), 7.66 (d, 1H, *J* = 9.6 Hz, 4-H), 7.52 (d, 1H, *J* = 8.4 Hz, 5-H), 7.01 (d, 1H, *J* = 8.4 Hz, 6-H), 6.37 (d, 1H, *J* = 9.6 Hz, 3-H), 3.46 (m, 2H, 1'-CH_2), 1.24 (t, 3H, *J* = 7.2 Hz, 2'-CH_3); ESI-MS (*m/z*): 285 $(M+H)^+$.

N-dodecyl-8-imino-2-oxo-2H,8H-pyrano[2,3-f] chromene-9-carboxamide (4c)

Brick red solid; yield: 60%; mp: 165–167 °C; IR (KBr): *v* 3427, 3212 (N–H), 2956, 2921, 2851, 1714 (C=O), 1678 (C=N), 1619 (C=O) cm^{-1}; ^1H NMR (400 MHz, $CDCl_3$): δ 10.00 (s, 1H, 12-NH), 9.01 (s, 1H, 10-H), 7.75 (brs, 1H, 8-NH), 7.66 (d, 1H, *J* = 9.6 Hz, 4-H), 7.52 (d, 1H, *J* = 8.8 Hz, 5-H), 7.03 (d, 1H, *J* = 8.8 Hz, 6-H), 6.40 (d, 1H, *J* = 9.6 Hz, 3-H), 3.43 (q, 2H, *J* = 7.2 Hz, 1'-CH_2), 1.25 (brs, 20H, 2'–11'-CH_2), 0.87 (t, 3H, *J* = 4.6 Hz, 12'-H); ESI-MS (*m/z*): 425 $(M+H)^+$.

N-cyclopropyl-8-imino-2-oxo-2H,8H-pyrano[2,3-f] chromene-9-carboxamide (4d)

Off white solid; yield: 77%; mp: 196–198 °C; IR (KBr): *v* 3452, 3314 (N–H), 3065, 2924, 1735 (C=O), 1677 (C=N),

1619 (C=O) cm^{-1}; ^1H NMR (400 MHz, $CDCl_3$): δ 10.04 (brs, 1H, 12-NH), 8.93 (s, 1H, 10-H), 7.69 (brs, 1H, 8-NH), 7.66 (d, 1H, J = 9.6 Hz, 4-H), 7.52 (d, 1H, J = 8.4 Hz, 5-H), 7.01 (d, 1H, J = 8.4 Hz, 6-H), 6.38 (d, 1H, J = 9.6 Hz, 3-H), 2.95 (m, 1H, 1'-H), 0.83 (m, 2H, 2',3'-H), 0.61 (m, 2H, 2',3'-H); ^{13}C NMR (100 MHz, $CDCl_3$): δ162.7 (C-2), 159.1 (C-8), 156.3 (C-11), 155.5 (C-6a), 151.4 (C-1a), 142.9 (C-4), 134.2 (C-5), 131.1 (C-10), 121.2 (C-10a), 115.6 (C-9), 114.6 (C-3), 111.9 (C-4a), 108.6 (C-6), 23.0 (C-1'), 6.6 (C-2',3'); ESI-MS (*m/z*): 297 $(M+H)^+$.

N-cyclohexyl-8-imino-2-oxo-2H,8H-pyrano[2,3-f]chromene-9-carboxamide (4e)

Pale yellow solid; yield: 85%; mp: 151–154 °C; IR (KBr): *v* 3535, 3228 (N–H), 3066, 2928, 2855, 1717 (C=O), 1675 (C=N), 1632 (C=O) cm^{-1}; ^1H NMR (400 MHz, $CDCl_3$): δ 10.01 (d, 1H, J = 6.8 Hz, 12-NH), 8.85 (s, 1H, 10-H), 7.73 (s, 1H, 8-NH), 7.66 (d, 1H, J = 9.6 Hz, 4-H), 7.51 (d, 1H, J = 8.8 Hz, 5-H), 7.00 (d, 1H, J = 8.8 Hz, 6-H), 6.35 (d, 1H, J = 9.6 Hz, 3-H), 3.96 (m, 1H, 1'-H), 1.95–1.22 (m, 10H, 2'–6'-CH_2); ^{13}C NMR (100 MHz, $CDCl_3$): δ 160.2 (C-2), 159.2 (C-8), 156.3 (C-11), 155.5 (C-6a), 151.3 (C-1a), 143.0 (C-4), 134.0 (C-5), 131.0 (C-10), 121.5 (C-10a), 115.4 (C-9), 114.5 (C-3), 111.9 (C-4a), 108.5 (C-6), 48.3 (C-1'), 32.8 (C-2'), 32.7 (C-6'), 25.7 (C-4'), 24.7 (C-3'), 24.5 (C-5'); ESI-MS (*m/z*): 339 $(M+H)^+$.

8-imino-9-(morpholine-4-carbonyl)-2H,8H-pyrano[2,3-f]chromen-2-one (4f)

Pale yellow solid; yield: 87%; mp: 143–146 °C; IR (KBr): *v* 3454, 3281 (N–H), 2984, 2925, 2855, 1740 (C=O), 1661 (C=N), 1621 (C=O) cm^{-1}; ^1H NMR (400 MHz, $CDCl_3$): δ 8.50 (s, 1H, 10-H), 7.81 (s, 1H, 8-NH), 7.68 (d, 1H, J = 9.6 Hz, 4-H), 7.49 (d, 1H, J = 8.4 Hz, 5-H), 7.02 (d, 1H, J = 8.4 Hz, 6-H), 6.39 (d, 1H, J = 9.6 Hz, 3-H), 3.78 (t, 4H, 3'-H_2, 5'-H_2), 3.72 (m, 2H, 2'-H, 6'-H), 3.47 (m, 2H, 2'-H, 6'-H); ESI-MS (*m/z*): 327 $(M+H)^+$.

N-benzyl-8-imino-2-oxo-2H,8H-pyrano[2,3-f]chromene-9-carboxamide (4g)

Pale yellow solid; yield: 83%; mp: 217–219 °C; IR (KBr): *v* 3452, 3305 (N–H), 3193, 3067, 1735 (C=O), 1677 (C=N), 1618 (C=O) cm^{-1}; ^1H NMR (400 MHz, $CDCl_3$): δ 10.43 (s, 1H, 12-NH), 9.02 (s, 1H, 10-H), 7.73 (s, 1H, 8-NH), 7.65 (d, 1H, J = 9.6 Hz, 4-H), 7.52 (d, 1H, J = 8.8 Hz, 5-H), 7.35 (m, 5H, 2'-H, 3'-H, 4'-H, 5'-H and 6'-H), 7.03 (d, 1H, J = 8.8 Hz, 6-H), 6.40 (d, 1H, J = 9.6 Hz, 3-H), 4.65 (d, 2H, J = 6.0 Hz, 13-CH_2); ^{13}C NMR (100 MHz, $CDCl_3$): δ 160.8 (C-2), 158.7 (C-8), 156.1 (C-11), 153.5 (C-6a), 142.7 (C-1a), 142.0 (C-4), 137.8 (C-5), 132.6 (C-10), 128.8 (C-3',5'), 127.9 (C-1'), 127.8 (C-2',6'), 127.6 (C-4'), 119.0 (C-10a), 116.5 (C-9), 115.2 (C-3), 113.0 (C-4a), 108.7 (C-6), 44.1 (C-13); ESI-MS (*m/z*): 347 $(M+H)^+$.

8-imino-2-oxo-N-(1-phenylethyl)-2H,8H-pyrano[2,3-f]chromene-9-carboxamide (4h)

Brick red solid; yield: 70%; mp: 174–176 °C; IR (KBr): *v* 3449, 3272 (N–H), 3067, 2932, 1738 (C=O), 1674 (C=N), 1617 (C=O) cm^{-1}; ^1H NMR (400 MHz, $CDCl_3$): δ 9.42 (s, 1H, 10-H), 9.16 (d, 1H, J = 7.6 Hz, 12-NH), 7.76 (s, 1H, 8-NH), 7.73 (d, 1H, J = 9.6 Hz, 4-H), 7.39–7.27 (m, 7H, 5-H, 6-H, 2'-H, 3'-H, 4'-H, 5'-H and 6'-H), 6.49 (d, 1H, J = 9.6 Hz, 3-H), 5.33–5.29 (m, 1H, 13-H), 1.61 (d, 3H, J = 6.8 Hz, 14-CH_3); ^{13}C NMR (100 MHz, $CDCl_3$): δ 160.5 (C-1'), 160.4 (C-2), 158.8 (C-8) 156.0 (C-11), 151.6 (C-6a), 142.8 (C-1a), 142.7 (C-4), 142.2 (C-5), 132.8 (C-10), 128.9 (C-3',5'), 127.6 (C-4'), 126.2 (C-2',6'), 118.6 (C-10a), 116.5 (C-9), 115.2 (C-3), 113.0 (C-4a), 108.6 (C-6), 49.9 (C-13), 22.4 (C-14); ESI-MS (*m/z*): 361 $(M+H)^+$.

N-benzhydryl-8-imino-2-oxo-2H,8H-pyrano[2,3-f]chromene-9-carboxamide (4i)

Off white solid; yield: 82%; mp: 197–199 °C; IR (KBr): *v* 3449, 3314 (N–H), 3063, 2925, 1734 (C=O), 1681 (C=N), 1619 (C=O) cm^{-1}; ^1H NMR (400 MHz, $CDCl_3$): δ 11.02 (s, 1H, 12-NH), 9.03 (s, 1H, 10-H), 7.75 (s, 1H, 8-NH), 7.65 (d, 1H, J = 9.6 Hz, 4-H), 7.53 (d, 1H, J = 8.6 Hz, 5-H), 7.33 (m, 10H, 2'-H, 3'-H, 4'-H, 5'-H, 6'-H and 2''-H, 3''-H, 4''-H, 5''-H, 6''-H), 7.05 (d, 1H, J = 8.6 Hz, 6-H), 6.45 (d, 1H, J = 8.4 Hz, 13-H), 6.40 (d, 1H, J = 9.6 Hz, 3-H); ESI-MS (*m/z*): 423 $(M+H)^+$.

8-imino-N-(1-(4-methoxyphenyl)ethyl)-2-oxo-2H,8H-pyrano[2,3-f]chromene-9-carboxamide (4j)

Pale yellow solid; yield: 65%; mp: 158–161 °C; IR (KBr): *v* 3451, 3318, 3279 (N–H), 3063, 1734 (C=O), 1679 (C=N), 1615 (C=O) cm^{-1}; ^1H NMR (400 MHz, $CDCl_3$): δ 10.43 (s, 1H, 12-NH), 8.94 (s, 1H, 10-H), 7.74 (brs, 1H, 8-NH), 7.64 (d, 1H, J = 9.6 Hz, 4-H), 7.50 (d, 1H, J = 8.8 Hz, 5-H), 7.31 (d, 2H, J = 8.4 Hz, 2'-H, 6'-H), 7.01 (d, 1H, J = 8.8 Hz, 6-H), 6.87 (d, 2H, J = 8.4 Hz, 3'-H, 5'-H), 6.37 (d, 1H, J = 9.6 Hz, 3-H), 5.23 (m, 1H, 13-H), 3.78 (s, 3H, 4'-OCH_3), 1.55 (d, 3H, J = 6.8 Hz, 14-CH_3); ^{13}C NMR (100 MHz, $CDCl_3$): δ 160.4 (C-2), 159.1 (C-8), 158.7 (C-4'), 156.4 (C-11), 155.5 (C-6a), 151.4 (C-1a), 142.9 (C-4), 135.8 (C-1'), 134.4 (C-5), 131.1 (C-10), 127.4 (C-2',6'), 121.3 (C-10a), 115.6 (C-9), 114.6 (C-3), 114.0 (C-3',5'), 111.9 (C-4a), 108.6 (C-6), 55.4 (4'-OCH_3), 49.0 (C-13), 22.6 (C-14); ESI-MS (*m/z*): 391 $(M+H)^+$.

N-(2,4-dimethoxybenzyl)-8-imino-2-oxo-2H,8H-pyrano[2,3-f]chromene-9-carboxamide (4k)

Pale yellow solid; yield: 89%; mp: 143–145 °C; IR (KBr): *v* 3449, 3272 (N–H), 3067, 2932, 1738 (C=O), 1674 (C=N), 1617 (C=O) cm^{-1}; ^1H NMR (400 MHz, $CDCl_3$): δ 10.34 (s, 1H, 12-NH), 8.97 (s, 1H, 10-H), 7.72 (brs, 1H, 8-NH), 7.63 (d, 1H, J = 9.6 Hz, 4-H), 7.49 (d, 1H, J = 8.8 Hz, 5-H), 7.25 (d, 1H, J = 8.4 Hz, 6'-H), 7.00 (d,

1H, J = 8.8 Hz, 6-H), 6.46 (s, 1H, 3'-H), 6.44 (d, 1H, J = 8.4 Hz, 5'-H), 6.37 (d, 1H, J = 9.6 Hz, 3-H), 4.56 (d, 2H, J = 5.6 Hz, 13-CH_2), 3.84 (s, 3H, 2'-OCH_3), 3.79 (s, 3H, 4'-OCH_3); ^{13}C NMR (100 MHz, $CDCl_3$): δ 160.5 (C-2), 159.2 (C-8), 158.7 (C-4'), 156.3 (C-11), 155.6 (C-2'), 151.4 (C-6a), 143.0 (C-1a), 142.9 (C-4), 134.0 (C-5), 130.9 (C-6'), 130.2 (C-10), 121.6 (C-1'), 118.5 (C-10a), 115.6 (C-9), 114.6 (C-3), 111.9 (C-4a), 108.5 (C-6), 103.9 (C-5'), 98.7 (C-3'), 55.5 (2',4'-OCH_3), 39.1 (C-13); ESI-MS (*m/z*): 407 $(M+H)^+$.

N-(2-bromobenzyl)-8-imino-2-oxo-2H,8H-pyrano [2,3-f]chromene-9-carboxamide (4l)

Brick red solid; yield: 82%; mp: 219–221 °C; IR (KBr): ν 3437, 3304 (N–H), 2924, 1755, 1736 (C=O), 1682 (C=N), 1617 (C=O) cm^{-1}; ^{1}H NMR (400 MHz, $CDCl_3$): δ 10.55 (s, 1H, 12-NH), 9.03 (s, 1H, 10-H), 7.79 (s, 1H, 8-NH), 7.66 (d, 1H, J = 9.6 Hz, 4-H), 7.56 (d, 1H, J = 8.8 Hz, 3'-H), 7.53 (d, 1H, J = 8.4 Hz, 5-H), 7.47 (d, 1H, J = 9.2 Hz, 6'-H), 7.30 (t, 1H, J = 8.8 Hz, 4'-H), 7.13 (t, 1H, J = 8.8 Hz, 5'-H), 7.03 (d, 1H, J = 8.4 Hz, 6-H), 6.40 (d, 1H, J = 9.6 Hz, 3-H), 4.72 (d, 2H, J = 6 Hz, 13-CH_2); ESI-MS (*m/z*): 427 $(M+H)^+$.

N-(3-bromobenzyl)-8-imino-2-oxo-2H,8H-pyrano [2,3-f]chromene-9-carboxamide (4m)

Orange red solid; yield: 72%; mp: 182–184 °C; IR (KBr): ν 3443, 3310 (N–H), 3068, 2924, 1741 (C=O), 1678 (C=N), 1618 (C=O) cm^{-1}; ^{1}H NMR (400 MHz, $CDCl_3$): δ 10.49 (s, 1H, 12-NH), 9.02 (s, 1H, 10-H), 7.75 (s, 1H, 8-NH), 7.66 (d, 1H, J = 9.4 Hz, 4-H), 7.54 (d, 1H, J = 8.4 Hz, 5-H), 7.49 (s, 1H, 2'-H), 7.39 (d, 1H, J = 8.1 Hz, 4'-H), 7.29 (d, 1H, J = 8.1 Hz, 6'-H), 7.20 (t, 1H, J = 8.1 Hz, 5'-H), 7.03 (d, 1H, J = 8.4 Hz, 6-H), 6.40 (d, 1H, J = 9.4 Hz, 3-H), 4.62 (d, 2H, J = 6 Hz, 13-CH_2); ^{13}C NMR (100 MHz, $CDCl_3$): δ 161.7 (C-2), 159.1 (C-8), 156.4 (C-11), 155.6 (C-6a), 151.5 (C-1a), 142.8 (C-1'), 140.8 (C-4), 135.0 (C-2'), 131.3 (C-4'), 130.7 (C-5), 130.5 (C-5'), 130.3 (C-10), 126.4 (C-6'), 122.8 (C-3'), 121.1 (C-10a), 115.7 (C-9), 114.7 (C-3), 111.9 (C-4a), 108.6 (C-6), 43.3 (C-13); ESI-MS (*m/z*): 427 $(M+H)^+$.

N-(2-chlorobenzyl)-8-imino-2-oxo-2H,8H-pyrano [2,3-f]chromene-9-carboxamide (4n)

Pale yellow solid; yield: 61%; mp: 222–224 °C; IR (KBr): ν 3451, 3311 (N–H), 3064, 1756, 1737 (C=O), 1682 (C=N), 1617 (C=O) cm^{-1}; ^{1}H NMR (400 MHz, $CDCl_3$): δ 10.54 (s, 1H, 12-NH), 9.02 (s, 1H, 10-H), 7.78 (s, 1H, 8-NH), 7.66 (d, 1H, J = 9.6 Hz, 4-H), 7.52 (d, 1H, J = 8.8 Hz, 5-H), 7.46 (dd, 1H, J = 7.4, 2.0 Hz, 3'-H), 7.37 (dd, 1H, J = 7.4, 2.0 Hz, 6'-H), 7.25–7.21 (m, 2H, 4'-H, 5'-H), 7.03 (d, 1H, J = 8.8 Hz, 6-H), 6.40 (d, 1H, J = 9.6 Hz, 3-H), 4.73 (d, 2H, J = 6.0 Hz, 13-CH_2); ESI-MS (*m/z*): 381 $(M+H)^+$.

N-(3-chlorobenzyl)-8-imino-2-oxo-2H,8H-pyrano [2,3-f]chromene-9-carboxamide (4o)

Pale yellow solid; yield: 65%; mp: 183–185 °C; IR (KBr): ν 3438, 3310 (N–H), 3065, 2923, 1740 (C=O), 1682 (C=N), 1620 (C=O) cm^{-1}; ^{1}H NMR (400 MHz, $CDCl_3$): δ 10.49 (s, 1H, 12-NH), 9.03 (s, 1H, 10-H), 7.75 (s, 1H, 8-NH), 7.67 (d, 1H, J = 9.6 Hz, 4-H), 7.54 (d, 1H, J = 8.4 Hz, 5-H), 7.34 (s, 1H, 2'-H), 7.24 (m, 3H, 4'-H, 5'-H and 6'-H), 7.04 (d, 1H, J = 8.4 Hz, 6-H), 6.40 (d, 1H, J = 9.6 Hz, 3-H), 4.63 (d, 2H, J = 5.6 Hz, 13-CH_2); ^{13}C NMR (100 MHz, $CDCl_3$): δ 161.7 (C-2), 159.1 (C-8), 156.4 (C-11), 155.6 (C-6a), 151.5 (C-1a), 142.8 (C-1'), 140.5 (C-4), 135.0 (C-3'), 134.6 (C-2'), 131.2 (C-6'), 130.0 (C-5), 127.8 (C-10), 127.6 (C-4'), 125.9 (C-5'), 121.1 (C-10a), 115.7 (C-9), 114.7 (C-3), 111.9 (C-4a), 108.6 (C-6), 43.4 (C-13); ESI-MS (*m/z*): 381 $(M+H)^+$.

N-(4-(tert-butyl)benzyl)-8-imino-4-methyl-2-oxo-2H,8H-pyrano[2,3-f]chromene-9-carboxamide (4p)

Pale yellow solid; yield: 68%; mp: 210–212 °C; IR (KBr): ν 3438, 3310 (N–H), 3065, 2923, 1740 (C=O), 1682 (C=N), 1620 (C=O) cm^{-1}; ^{1}H NMR (400 MHz, $CDCl_3$): δ 10.39 (s, 1H, 12-NH), 8.99 (s, 1H, 10-H), 7.72 (s, 1H, 8-NH), 7.64 (d, 1H, J = 9.6 Hz, 4-H), 7.51 (d, 1H, J = 8.4 Hz, 5-H), 7.37 (d, 2H, J = 8.4 Hz, 2'-H, 6'-H), 7.30 (d, 2H, J = 8.4 Hz, 3'-H, 5'-H), 7.02 (d, 1H, J = 8.4 Hz, 6-H), 6.38 (d, 1H, J = 9.6 Hz, 3-H), 4.62 (d, 2H, J = 5.6 Hz, 13- CH_2), 1.31 (s, 9H, 4'-$C(CH_3)_3$); ^{13}C NMR (100 MHz, $CDCl_3$): δ 161.5 (C-2), 159.1 (C-8), 156.3 (C-11), 155.6 (C-6a), 151.5 (C-1a),150.3 (C-4'), 142.9 (C-4), 135.3 (C-1'), 134.6 (C-5), 131.1 (C-10), 127.5 (C-2',6'), 125.6 (C-3',5'), 121.3 (C-10a), 115.6 (C-9), 114.7 (C-3), 111.9 (C-4a), 108.6 (C-6), 43.7 (C-13), 34.6 (3'-$\underline{C}(CH_3)_3$), 31.4 (3'-C($\underline{C}H_3)_3$); ESI-MS (*m/z*): 403 $(M+H)^+$.

8-imino-N-(2-(2-methoxyphenoxy)ethyl)-2-oxo-2H,8H-pyrano[2,3-f]chromene-9-carboxamide (4q)

Off white solid; yield: 87%; mp: 145–148 °C; IR (KBr): ν 3452, 3313 (N–H), 3067, 2922, 1729 (C=O), 1681 (C=N), 1618 (C=O) cm^{-1}; ^{1}H NMR (400 MHz, $CDCl_3$): δ 10.41 (s, 1H, 12-NH), 8.99 (s, 1H, 10-H), 7.80 (s, 1H, 8-NH), 7.67 (d, 1H, J = 9.6 Hz, 4-H), 7.53 (d, 1H, J = 8.4 Hz, 5-H), 7.03 (d, 1H, J = 8.4 Hz, 6-H), 6.94 (m, 4H, 3'-H, 4'-H, 5'-H, 6'-H), 6.40 (d, 1H, J = 9.6 Hz, 3-H), 4.22 (t, 2H, 14-H), 3.89 (m, 2H, 13-H), 3.87 (s, 3H, 2'-OCH_3); ESI-MS (*m/z*): 407 $(M+H)^+$.

Determination of AChE and BuChE inhibitory activities

Inhibitory potency of target compounds against AChE and BuChE were assayed using spectrophotometric method developed by Ellman *et al.* (31) with slight modification. In brief, reaction mixture composed of 10 μL of test sample of five different concentrations, 145 μL phosphate buffer 200 mM (pH 7.7), 80 μL of dithiobisnitrobenzoic acid (DTNB) (18.5 mg of DTNB dissolved in 10 mL phosphate

buffer pH 7.7), and 10 μL of enzyme (0.4 U/mL). The mixture was incubated at 25 °C for 5 min. Subsequently, the enzymatic reaction was initiated by addition of 15 μL of 1 mM of acetylthiocholine iodide or butyrylthiocholine iodide (according to the respective enzyme), and the mixture was again incubated for 5 min at 25 °C. The rate of absorbance change was measured at 412 nm for 6 min using a microplate reader (Bio-Rad 680, Germany). Galantamine was applied as positive drug.

In vitro *antioxidant activity assay*

The radical scavenging activity of the test compounds was measured by the ABTS method (32). The ABTS was dissolved in water to obtain an 8 mM concentration of ABTS stock solution. ABTS radical cation ($ABTS^{\bullet+}$) was generated by adding 3 mM potassium persulfate to the ABTS stock solution and keeping it in the dark at room temperature for 12–18 h. The $ABTS^{\bullet+}$ solution was diluted with ethanol to give an absorbance of 0.48 ± 0.07 at 734 nm. The 10 μL of the test compounds were allowed to react with 290 μL of $ABTS^{\bullet+}$ solution. The absorbance was taken 30 min after initial mixing. Trolox was used as a standard.

ThT fluorescence assay

The acceleration activity of synthetic analogs on $A\beta_{1-42}$ aggregation was determined using ThT fluorescence assay (33). The accelerating $A\beta_{1-42}$ (Sigma) was dissolved in DMSO to make a 200 μM stock solution. The stock solution was centrifuged at the speed of 13 500 × g for 10 min. The above supernatant was used for experiments. The most active compound **4m** was dissolved in DMSO at concentrations of 0.02, 0.06, 0.1 mM. Further, the binding and modulating ability of **4m** was ascertained by the most widely used method thioflavin T (ThT) assay, to identify Aβ fibrils with high sensitivity. Test compound **4m** (2 μL) (in concentrations of 0.02–0.1 mM) and 2 μL of 200 mM Aβ42 were added into 76 μL of phosphate-buffered saline (PBS at pH 7.4). After incubation for 24 h at room temperature, 80 μL of 5 μM ThT solution (in 50 mM glycine-NaOH at pH 8.5) was added to the reaction solution. Fluorescence emission spectra measurements were carried out on Perkin Elmer LS55 fluorescence spectrometer within the range from 410 to 600 nm, with an excitation wavelength of 390 nm. Identical spectra were recorded by performing the independent experiments thrice.

Kinetic study

To obtain estimates of the inhibition model and inhibition constant Ki, reciprocal plots of 1/V versus 1/[S] were constructed at different concentrations of the substrate acetylthiocholine iodide (0.1–0.5 mM) using Ellman's method. The assay solution (250 μL) consists of 145 μL of 200 mM phosphate buffer (pH 7.7), with the addition of 80 μL of DTNB (18.5 mg of DTNB dissolved in 10 mL phosphate buffer pH 7.7), 10 μL of 0.4 units/mL AChE, and 15 μL of substrate (ATCh). Three different concentrations of inhibitors (5, 10, and 30 nM) were added to the assay solution and preincubated for 5 min at 25 °C with the AChE followed by the addition of substrate in different concentrations. The parallel control experiments were performed without inhibitor in the assay. Progress curves were monitored at 412 nm over 6 min. Then, double reciprocal plots (1/v versus 1/[s]) were constructed using GraphPad prism version 5 (34). The re-plots of the slopes and intercepts of the double reciprocal plots against inhibitor concentrations gave the inhibitor constants (K_{i1} and K_{i2}, for the binding to free enzyme and enzyme substrate complex) as the intercepts on the *x*-axis. Data analysis was performed using Microsoft Excel.

Molecular Docking study

Molecular docking studies were performed using SCHRÖDINGER MAESTRO software (version 9.2; Schrödinger LLC, New-York, NY, USA). The protein used for docking is the crystal structure of electric eel acetylcholinesterase (*Ee*AChE, PDB ID: 1C2O) after eliminating the original inhibitors and water molecules. The ligands used as inputs for docking were designed using CHEMBIOOFFICE 2010 software and prepared using LIGPREP [version 2.5, Schrödinger Inc., Schrödinger maestro software (version 9.2; Schrödinger LLC, New York, USA)]. GLIDE (grid-based ligand docking with energetics) module of Schrodinger was used for the docking studies. A grid was generated around the active site of the enzyme by specifying the key active site residues: D74, T83, W86, G120, G121, G122, Y124, Y133, E202, S203, W286, F295, F297, Y337, and Y341. The poses generated per ligand were set to 10 000, and the pose chosen for energy minimization was set to 10. Glide docking score was used to determine the best docked structure from the output (35).

Results and Discussion

Chemistry

As illustrated in Scheme 1, the target compounds **4a**–**q** could be prepared in economical way using inexpensive materials in four steps starting from resorcinol. At first stage, 7-hydroxycoumarin (**1**) was prepared by using Pechmann condensation between resorcinol and DL-malic acid in the presence of conc. H_2SO_4 (26). Then, the obtained **1** was treated with HMTA in acetic acid to gain 7-hydroxy-8-formylcoumarin (**2**) by Duff formylation (27). Readily available ethylcyanoacetate was reacted with a series of appropriate amines to give the corresponding N-substituted cyanoacetamide derivatives (**3a**–**q**) according to reported procedures (28,29). Finally, the different N-substituted cyanoacetamides and **2** underwent intramolecular cyclization with Et_3N to yield desired prototypes (30). All synthesized compounds **4a**–**q** were characterized by mass analysis and IR, ^1H, and ^{13}C NMR spectroscopy. The IR spectra of compounds showed absorption bands of =N–H and C=N stretching vibrations at 3535–3427 cm^{-1} and 1661–1683 cm^{-1}, respectively. The characteristic strong

bands appeared for C=O stretching in coumarin at 1714–1746 cm^{-1}. The ^{1}H NMR spectra of all the compounds showed singlet of the imino group proton resonated at 7.69–7.81 ppm and the heterocyclic ring protons of coumarin resonated as two doublets between 6.35–6.49 and 7.63–7.73 ppm. In the ^{13}C NMR spectra, the carbon resonance frequencies of the C=O of coumarin was at 160.2–162.7 ppm and C=O of amide at 156.0–156.4 ppm. These data confirmed the formation of extended iminopyran ring on coumarin moiety by the reaction between –CHO, –OH, and –CN groups. Moreover, their ESI-MS spectra showed molecular ion $(M+H)^{+}$ peaks further confirming their structure. All spectroscopic measurements confirmed the structure and high purity of synthesized compounds.

In vitro *inhibition of cholinesterase*

To determine the therapeutic potential of target tricyclic fused coumarin derivatives in the treatment of AD, the inhibitory activities of compounds **4a**–**q** together with reference compound galantamine against both AChE and BuChE was evaluated according to Ellman's protocol by measuring the rate of acetylthiocholine or butyrylthiocholine hydrolysis in the presence of the inhibitor. All compounds proved to be remarkably active toward AChE in the low nanomolar range of IC_{50} values and almost inactive on BuChE revealed an extremely selective inhibitory profile for this series of compounds. The anti-AChE activities of the target compounds are summarized in Table 1 as IC_{50} values. From the data, it is notable that among the seventeen compounds tested, six analogs exhibited 4- to 51-fold higher inhibitory activity toward AChE than galantamine, a standard drug. The other ten analogs have shown the better to comparable potency to that of galantamine, while only **4d** was less active. Although the activity of compound **4d** was less than standard drug galantamine, but it had a fairly good inhibitory activity. Compound **4m**, which has *N*-(3-bromobenzyl)amide moiety, exhibited superior anti-AChE activity with IC_{50} value of 13 ± 1.4 nM in this series which is 51-fold more potent than galantamine. The changes of substituents on the terminal amide moiety evidently influence AChE inhibitory effect of target compounds. Elongation of aliphatic chain on N of amide increased the activity due to the more lipophilic property of these substituents. It is worthwhile to note that **4d** with cyclopropyl amide moiety showed the most dramatic activity loss relative to compounds with straight chain alkyl groups on N of amide as in **4a**, **4b**, and **4c**. Mutation of this moiety from cyclopropylamido to cyclohexylamido improved the activity by 4.7 times. Meanwhile, changing alkyl amide to alkylaryl amide moiety led to a huge decrease in activity. However, the substituent position on the aromatic ring could largely affect the activity of the target compounds. The electron withdrawing substituents such as bromo and chloro at position 2 and 3 increased the inhibitory activity by 5.6- to 38.2-fold as seen in compounds **4l**, **m**, **n**, and **o**. On the other hand, electron donating groups such as methoxy at positions 2 and 4 induce their enhancing effects as seen in **4j** and **k**. Comparing to the unsubstituted counterpart **4g**, analog bearing 4-*ter*-butyl-substituted benzylamido (**4p**) displayed approximately four-fold stronger activity.

Table 1: Acetylcholinesterase inhibitory and ABTS radical scavenging activities of synthetic 8-imino-2-oxo-2*H*,8*H*-pyrano[2,3-*f*]chromene-based compounds **4a**–**q** and reference compounds

	IC_{50} ± SEM[a]	
Compounds	AChE[b] (nm)	ABTS radical scavenging activity (μm)
4a	415 ± 30.44	>50
4b	259 ± 9.71	29.82 ± 0.74
4c	83 ± 3.2	>50
4d	799 ± 31.88	24.35 ± 1.64
4e	169 ± 15.5	19.59 ± 1.23
4f	226 ± 16.74	11.19 ± 0.98
4g	497 ± 40.50	10.79 ± 1.05
4h	462 ± 36.03	>50
4i	669 ± 47.89	26.24 ± 1.59
4j	390 ± 24.34	14.81 ± 0.81
4k	300 ± 25.38	15.24 ± 1.41
4l	27 ± 2	>50
4m	13 ± 1.4	>50
4n	30 ± 2	48.16 ± 1.48
4o	88 ± 7.5	41.40 ± 3.75
4p	77 ± 4.5	22.34 ± 1.58
4q	440 ± 31	28.35 ± 0.7
Galantamine	665 ± 20.20	–
Trolox	–	27.35 ± 1.34

[a]Concentration required to produce 50% inhibition of enzyme activity. IC_{50} values are given as the mean of three independent determinations.
[b]AChE from electric eel.

Enzyme Kinetic studies

The mechanism involved in the AChE inhibition by these fused coumarins was investigated using compound **4m**, the most potent *Ee*AChE inhibitor (Table 1). For this purpose, the rate of the enzyme activity was measured at four different concentrations of compound **4m** (0, 5, 10, and 30 nM) using different concentration of the substrate acetylthiocholine (ATCh). In each case, the initial velocity was measured at different concentrations of the substrate (S), and the reciprocal of the initial velocity (1/v) was plotted against the reciprocal of [ATCh]. The graphical presentation of steady state inhibition data of **4m** for AChE is shown Figure 1. The results revealed that there was an increasing slope and increasing intercept at higher inhibitor concentrations, indicating a mixed-type inhibitory ability for **4m**. This behavior was also indicated by intersection of double reciprocal lines in the upper left quadrant of Lineweaver–Burk plot. Generally, this type of inhibition indicates dual binding site mode of interactions by binding to both the CAS and PAS of AChE. The inhibition constants K_{i1} and K_{i2} obtained were 11.84 nM and 25.91 nM.

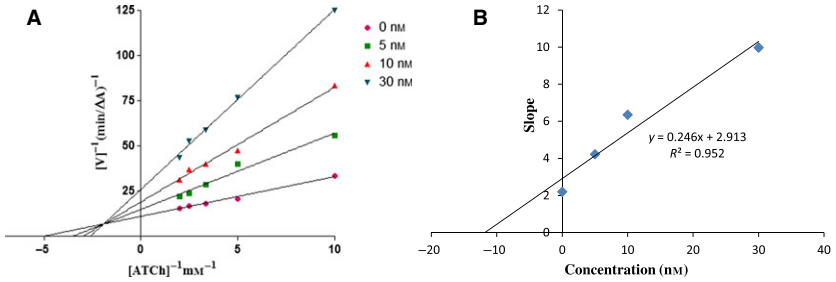

Figure 1: Kinetic study on the mechanism of EeAChE inhibition by compound **4m**. (A) Lineweaver–Burk plot of reciprocal of initial velocities versus reciprocal of acetylthiocholine iodide concentrations (0.1–0.5 mM) in the absence and presence of **4m** at 5, 10, and 30 nM; (B) secondary plots of the Lineweaver–Burk plot, slope versus various concentrations of **4m**.

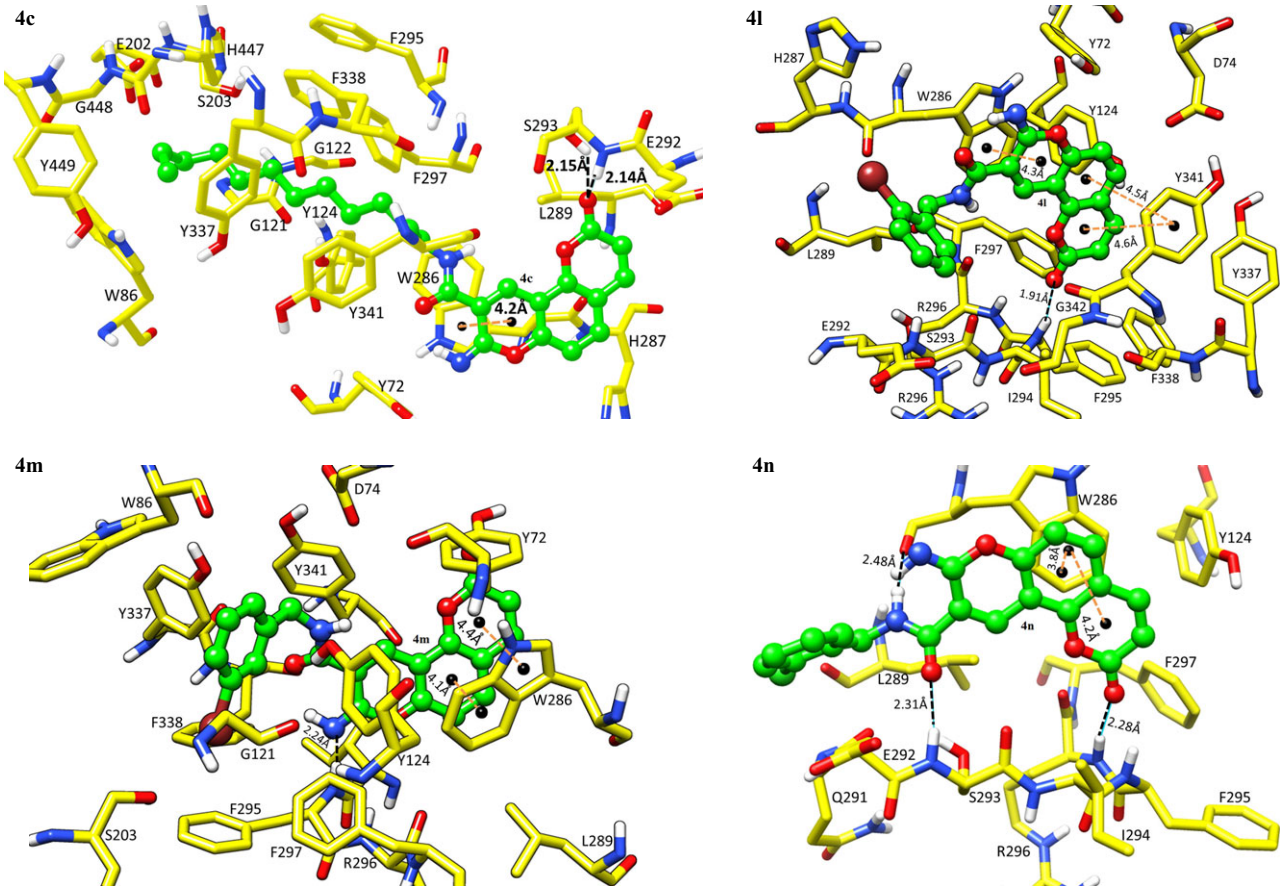

Figure 2: Best ranked binding orientation of most active compounds **4c**, **4l**, **4m**, and **4n** (in green color) in the binding site of AChE enzyme. The hydrogen bonds and π-π interactions are shown as bold black and orange dashed lines, respectively.

Molecular docking study

To further study the interaction mode of fused tricyclic coumarin derivatives with respect to AChE, ligand docking studies were performed on active compounds using Schrödinger maestro software (version 9.2; Schrödinger LLC, NewYork) based on the 3D structure of the electric eel enzyme complex (*Ee*AChE, PDB ID: 1C2O). The best docked poses in terms of glide energy of binding were further analyzed to clarify interactions between ligands and the enzyme. An overall view of docking poses of **4c**, **4l**, **4m**, and **4n** with respect to the key residues in the binding site is depicted in Figure 2.

The results of docking revealed that all of these compounds exhibit multiple binding modes with AChE. At the entrance of the enzyme, π-π stacking interactions between fused tricyclic coumarin moiety and indole ring of PAS residue Trp286 is a common feature of all docked

compounds. This feature of the molecules takes part in recognition and orientation of the ligands in the active site. This interaction is able to attribute two orientations to these compounds so that the substituted benzyl amide or alkyl amide moiety at position 9 is extended either into the CAS or out from the active site gorge. It was therefore concluded that the coumarin parts of the molecules are accommodated in the gorge rim, while amide fragment is oriented toward the CAS or outwards the active site.

The binding poses of **4l** and **4p** places the ligand PAS region and sandwiched the fused tricyclic coumarin moiety between Trp286 and Tyr341 residues by π-π stacking with the ring–ring distance in the range of 4.3–4.7 Å similar to that observed in known inhibitor tacrine. Oxygen of the carbonyl group of coumarin moiety forms a hydrogen bond interaction with the backbone -NH group of Phe295. Consequently, 2-bromobenzylamide (**4l**) and 4-t-butylbenzylamide (**4p**) moieties extended out from the active gorge by forming hydrophobic interactions with Leu289, His287, Ser293, and Glu292 at gorge rim.

The most energetically favored binding mode for compounds **4c**, **4m**, and **4o** inverse to that of **4l** and places the ligand in the PAS with the fused tricyclic coumarin moiety stacking with Trp286 residue and the substituted benzyl or alkyl amide moiety leaning toward the CAS by forming hydrophobic interactions with Trp86, Glu121, His447, Ser203, and Tyr337 residues which resembles with those observed for known inhibitor donepezil. In this orientation, the nitrogen of the iminopyran moiety of **4m** and **4o** establishes hydrogen bond interaction with the -NH group of Phe295 and Arg296, respectively. In case of **4c**, the carbonyl group of coumarin moiety is involved in bifurcated hydrogen bond interactions with -NH (2.14 Å) and -OH (2.15 Å) of Ser 293. The long aliphatic chain in **4c** was found to be entered deep into the gorge showing interactions with the catalytic triad residues as that observed in galantamine and rivastigmine. This binding mode is in agreement with mixed-type inhibition pattern of **4c**, **4m**, and **4o** in which ligand simultaneously bind to CAS and PAS of AChE. From the above observations, it is understood that the compound **4m** could act as a potent dual binding site inhibitor of AChE.

A close examination into the docking mode of **4n** reveals hydrogen bond interactions between the carbonyl group of coumarin moiety and -NH group of Arg296, and from the carbonyl and -NH groups of amide fragment to Ser 293 and Trp286, respectively. The tricyclic coumarin moiety interacts with Trp286 by means of a π-π stacking as in **4o** and the 3-chlorobenzylamide moiety extended out from the active site gorge as in **4l**. Therefore, the higher potency of these tricyclic coumarin compounds with N-benzyl/alkyl carboxamide could be due to the more favorable interactions of compounds with the target enzyme.

In vitro *antioxidant activity*

The reduction of the oxidative stress is another crucial aspect in designing agents for AD treatment. The antioxidant capacity of coumarin derivatives **4a**–**q** were examined using the well-established ABTS (2,2'-azino-bis(3-ethylbenzthiazoline-6-sulfonic acid)) radical scavenging method in comparison with trolox, a water-soluble vitamin E analog. The ability of compounds to scavenge ABTS radicals was shown as IC_{50}, the test compound's concentration resulting in 50% inhibition of free radical (Table 1). The data showed that ten synthetic derivatives demonstrated potent ABTS radical scavenging capacities in the range of 10.79–29.82 μM. Among them, five compounds had higher antioxidant activities ranging from 1.4- to 2.5-fold of trolox. Among all seventeen analogs, only five displayed poor antioxidant activities, with IC_{50} values >50 μM.

Effect on the Aβ aggregation

Reducing the neuronal cytotoxicity of amyloid peptides by accelerating the aggregation process, which is different from prevalent methods via inhibiting the aggregation of peptides, is another crucial aspect in the development of anti-AD agents (18). Thioflavin T (ThT) assay is one of the most widely used methods to identify Aβ aggregates with high sensitivity (36). The emission band at 450 nm is expected to be directly proportional to the amount of Aβ aggregates present; consequently, the formation of Aβ aggregates can be easily followed by measuring ThT fluorescence enhancement by organic molecules in concentration-dependent manner (19). To investigate the effect of the synthesized analogs on Aβ aggregation, compound **4m** (0.02, 0.06, 0.1 mM), which showed good activity in former tests, and galantamine were selected to perform thioflavin T (ThT) assay. After the addition of **4m**

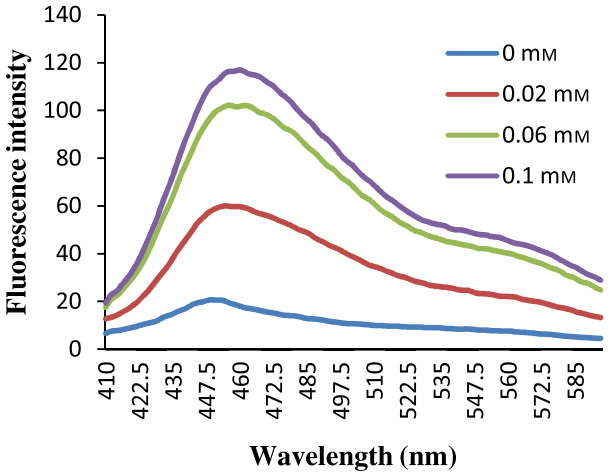

Figure 3: Detection of Aβ aggregates using ThT assay; fluorescence enhancement spectra (λ_{ex} = 390 nm, λ_{em} = 450 nm) of 80 μL of 5 μM ThT solution (in 50 mM glycine-NaOH at pH 8.5) mixed in 2 μL of 200 mM $A\beta_{1-42,}$ with different concentrations (0.02, 0.06, 0.1 mM) of **4m** was measured after 24 h of incubation time.

to Aβ_{1-42} aqueous solution and incubation for 24 h, a gradual enhancement in the fluorescence intensity of ThT at 450 nm was observed which is indicative of dosage-dependent manner of the acceleration of Aβ_{1-42} aggregation (Figure 3). As for galantamine, no significant enhancement in fluorescence was observed no matter low or high concentration of galantamine was used. Clearly, in comparison with galantamine, compound **4m** showed additional acceleration of Aβ_{1-42} aggregation process, which may alleviate the Aβ-induced toxicity and eventually benefit the treatment of AD.

Conclusion

In summary, a series of new fused tricyclic coumarins bearing N-alkyl/alkylaryl amide moieties were synthesized and evaluated for AChE and BuChE inhibitory activity using a modified Ellman's method. The results showed that most of the target compounds exhibited exclusively potent anti-AChE activity. Among the seventeen coumarin analogs, compound **4m** with an *N*-(3-bromobenzyl) amide pendent group displayed highest AChE inhibitory activity (IC_{50} 13 ± 1.4 nM) of 51-fold superior to galantamine. These synthetic derivatives also exhibited potent ABTS radical scavenging activity in an antioxidant assay. Surprisingly, the most potent analog **4m** displayed dosage-dependent acceleration of Aβ_{1-42} aggregation, which may convert the Aβ monomers and oligomers into non-toxic forms because the oligomeric forms of amyloid peptides are reported to have higher toxicity as compared to the fibrillar aggregates. Both the inhibition kinetic analysis and molecular docking studies demonstrated that **4m** showed a mixed-type inhibition, interacting simultaneously with both CAS and PAS of AChE, and inducing a strong dual binding site inhibition of the enzyme. Moreover, based on the docking studies, it was suggested that the complex of ligand and protein in the active site is stabilized through π-π stacking and hydrogen bond interactions. Data from these studies could give the definitive proof of concept of the potential of these coumarin derivatives as a multipotent hit molecule for the treatment of AD.

Acknowledgments

This work was supported by start-up grant (SR/FT/CS-60/2010) from Department of Science and Technology (DST), New Delhi, India. The authors thank Dr. S. Rajagopal for the support in fluorescence assay. Authors also thank Dr. R.V. Jayanth Kasyap for critical reading and improving the manuscript.

Conflict of Interest

The authors confirm that this article content has no financial or commercial conflict of interests.

References

1. Luengo-Fernandez R., Leal J., Gray A.M. (2011) Cost of dementia in the pre-enlargement countries of the European Union. J Alzheimers Dis;27:187–196.
2. Palmer M. (2011) Neuroprotective therapeutics for Alzheimer's disease: progress and prospects. Trends Pharmacol Sci;32:141–147.
3. Prince M., Wimo A., Guerchet M., Claire Ali G., Wu Y.T., Prina M. (2015) Alzheimer's Disease International World Alzheimer Report 2015. 1–82.
4. Terry A.V., Buccafusco J.J. (2003) The cholinergic hypothesis of age and Alzheimer's disease-related cognitive deficits: recent challenges and their implications for novel drug development. J Pharmacol Exp Ther;306:821–827.
5. Bores G.M., Huger F.P., Petko W., Mutlib A.E., Camacho F., Rush D.K., Selk D.E., Wolf V., Kosley R.W. Jr, Davis L., Vargas H.M. (1996) Pharmacological evaluation of novel Alzheimer's disease therapeutics: acetylcholinesterase inhibitors related to galanthamine. J Pharmacol Exp Ther;277:728–738.
6. Ansari M.A., Scheff S.W. (2010) Oxidative stress in the progression of Alzheimer disease in the frontal cortex. J Neuropathol Exp Neurol;69:155–167.
7. Thiratmatrakul S., Yenjai C., Waiwut P., Vajragupta O., Reubroycharoen P., Tohda M., Boonyarat C. (2014) Synthesis, biological evaluation and molecular modeling study of novel Tacrine-carbazole hybrids as potential multifunctional agents for the treatment of Alzheimer's disease. Eur J Med Chem;75:21–30.
8. Selkone D.J. (1997) Alzheimer's disease: genotypes, phenotypes, and treatments. Science;275:630–631.
9. Chiti F., Dobson C.M. (2006) Protein misfolding, functional amyloid, and human disease. Annu Rev Biochem;75:333–366.
10. LaFerla F.M., Green K.N., Oddo S. (2007) Intracellular amyloid-beta in Alzheimer's disease. Nat Rev Neurosci;8:499–509.
11. Roychaudhuri R., Yang M., Hoshi M.M., Teplow D.B. (2009) Amyloid β-protein assembly and Alzheimer disease. J Biol Chem;284:4749–4753.
12. Hamley I.W. (2012) The amyloid beta peptide: a chemist's perspective. Role in Alzheimer's and fibrillization. Chem Rev;112:5147–5192.
13. Takahashi T., Mihara H. (2008) Peptide and protein mimetics inhibiting amyloid beta-peptide aggregation. Acc Chem Res;41:1309–1318.
14. McLaurin J., Cecal R., Kierstead M.E., Tian X., Phinney A.L., Manea M., French J.E. *et al.* (2002) Therapeutically effective antibodies against amyloid-beta peptide target amyloid-beta residues 4–10 and inhibit cytotoxicity and fibrillogenesis. Nat Med;8:1263–1269.
15. Hindo S.S., Mancino A.M., Braymer J.J., Liu Y., Vivekanandan S., Ramamoorthy A., Lim M.H. (2009) Small molecule modulators of copper-induced Aβ aggregation. J Am Chem Soc;131:16663–16665.

16. Cavalli A., Bolognesi M.L., Capsoni S., Andrisano V., Bartolini M., Margotti E., Cattaneo A., Recanatini M., Melchiorre C.A. (2007) Small molecule targeting the multifactorial nature of Alzheimer's disease. Angew Chem Int Ed;46:3689–3692.
17. Cabaleiro-Lago C., Quinlan-Pluck F., Lynch I., Lindman S., Minogue A.M., Thulin E., Walsh D.M., Dawson K.A., Linse S. (2008) Inhibition of amyloidβ protein fibrillation by polymeric nanoparticles. J Am Chem Soc;130:15437–15443.
18. Liu L., Zhang L., Niu L., Xu M., Mao X., Yang Y., Wang C. (2011) Observation of reduced cytotoxicity of aggregated amyloidogenic peptides with chaperone-like molecules. ACS Nano;5:6001–6007.
19. Muthuraj B., Chowdhury S.R., Iyer P.K. (2015) Modulation of Amyloid-β fibrils into mature microrod-shaped structure by histidine functionalized water-Soluble perylene diimide. ACS Appl Mater Interfaces;7:21226–21234.
20. Anand P., Singh B., Singh N. (2012) A review on coumarins as acetylcholinesterase inhibitors for Alzheimer's disease. Bioorg Med Chem;20:1175–1180.
21. Alipour M., Khoobi M., Moradi A., Nadri H., Moghadam F.H., Emami S., Hasanpour Z., Foroumadi A., Shafiee A. (2014) Synthesis and anti-cholinesterase activity of new 7- hydroxycoumarin derivatives. Eur J Med Chem;83:536–544.
22. Asadipour A., Alipour M., Jafari M., Khoobi M., Emami S., Nadri H., Sakhteman A., Moradi A., Sheibani V., Moghadam F.H., Shafiee A., Foroumadi A. (2013) Novel coumarin-3 carboxamides bearing N-benzylpiperidine moiety as potent acetylcholinesterase inhibitors. Eur J Med Chem;70:623–630.
23. Catto M., Pisani L., Leonetti F., Nicolotti O., Pesce P., Stefanachi A., Cellamare S., Carotti A. (2013) Design, synthesis and biological evaluation of coumarin alkylamines as potent and selective dual binding site inhibitors of acetylcholinesterase. Bioorg Med Chem;21:146–152.
24. Alipour M., Khoobi M., Foroumadi A., Nadri H., Moradi A., Sakhteman A., Ghandi M., Shafiee A. (2012) Novel coumarin derivatives bearing N-benzyl pyridinium moiety: potent and dual binding site acetylcholinesterase inhibitors. Bioorg Med Chem;20:7214–7222.
25. Kontogiorgis C.A., Xu Y., Hadjipavlou-Litina D., Luo Y. (2007) Coumarin derivatives protection against ROS production in cellular models of Abeta toxicities. Free Radic Res;41:1168.
26. Pechmann H.V., Duisberg C. (1893) Synthesis of coumarins by condensation of phenols with beta keto ester in presence of Lewis acid catalysts. Berichte;16:2119.
27. Bender D.R., Kanne D., Frazier J.D., Rapoport H. (1983) Synthesis and derivatization of 8-acetylpsoralens. Acetyl migrations during Claisen rearrangement. J Org Chem;48:2709–2719.
28. Wang K., Nguyen K., Huang Y., Domling A. (2009) Cyanoacetamide multicomponent reaction (I): parallel synthesis of cyanoacetamides. J Comb Chem;11:920.
29. Tamiz P., Cai S.X., Zhou Z.L., Yuen P.W., Schelkun R.M., Whittemore E.R., Weber E., Woodward R.M., Keana J.F.W. (1999) Structure-activity relationship of N-(phenylalkyl)cinnamides as novel NR2B subtype-selective NMDA receptor antagonists. J Med Chem;42:3412.
30. Volmajer J., Toplak R., Lebanb I., Le A.M. (2005) Marechala, Synthesis of new iminocoumarins and their transformations into N-chloro and hydrazono compounds. Tetrahedron;61:7012–7021.
31. Ellman G.L., Courtney K.D., Andres V., Featherstone R.M. (1961) A new and rapid Colorimetric determination of acetylcholinesterase activity. Biochem Pharmacol;7:88–95.
32. Miller N.J., Rice-Evans C.A. (1997) Factors influencing the antioxidant activity determined by the ABTS^{d+} radical cation assay. Free Radic Res;26:195–199.
33. Fang L., Fang X., Gou S., Lupp A., Lenhardt I., Sun Y., Huang Z., Chen Y., Zhang Y., Fleck C. (2014) Design, synthesis and biological evaluation of D-ring opened galantamine analogs as multifunctional anti-Alzheimer agents. Eur J Med Chem;76:376–386.
34. Rampa A., Bisi A., Belluti F., Gobbi S., Valenti P., Andrisano V., Cavrini V., Cavalli A., Recanatini M. (2000) Acetylcholinesterase inhibitors for potential use in Alzheimer's disease: molecular modeling, synthesis and kinetic evaluation of 11H-indeno-[1,2-b]-quinolin-10- ylamine derivatives. Bioorg Med Chem;8:497–506.
35. Friesner R.A. (2004) *Glide:* a new approach for rapid, accurate docking and scoring. 1. Method and assessment of docking accuracy. J Med Chem;47:1739–1749.
36. Ma Q., Wei G., Yang X. (2013) Influence of Au nanoparticles on the aggregation of amyloid-β-(25−35) peptides. Nanoscale;5:10397–10403.

Supporting Information

Additional Supporting Information may be found in the online version of this article:

Appendix S1. Spectra for selected compounds.